Jan *et al. Soft Sci* 2024;4:10
DOI: 10.20517/ss.2023.54

Soft Science

Research Article

Open Access

Check for updates

A skin-wearable and self-powered laminated pressure sensor based on triboelectric nanogenerator for monitoring human motion

Agha Aamir Jan[#], Seungbeom Kim[#], Seok Kim[*]

Department of Mechanical Engineering, Pohang University of Science and Technology (POSTECH), Pohang 37673, Republic of Korea.
[#]Authors contributed equally.

[*]**Correspondence to:** Prof. Seok Kim, Department of Mechanical Engineering, Pohang University of Science and Technology (POSTECH), 77 Cheongam-Ro, Pohang 37673, Republic of Korea. E-mail: seok.kim@postech.ac.kr

How to cite this article: Jan AA, Kim S, Kim S. A skin-wearable and self-powered laminated pressure sensor based on triboelectric nanogenerator for monitoring human motion. *Soft Sci* 2024;4:10. https://dx.doi.org/10.20517/ss.2023.54

Received: 24 Nov 2023 **First Decision:** 8 Dec 2023 **Revised:** 11 Dec 2023 **Accepted:** 22 Dec 2023 **Published:** 26 Jan 2024

Academic Editor: Zhifeng Ren **Copy Editor:** Pei-Yun Wang **Production Editor:** Pei-Yun Wang

Abstract

Flexible and skin-wearable triboelectric nanogenerators (TENGs) have emerged as promising candidates for self-powered tactile and pressure sensors and mechanical energy harvesters due to their compatible design and ability to operate at low frequencies. Most research has focused on improving tribo-negative materials for flexible TENGs, given the limited options for tribo-positive materials. Achieving biocompatibility while maintaining the sensitivity and capability of energy harvesting is another critical issue for wearable sensors. Here, we report a TENG-based biocompatible and self-powered pressure sensor by simple fabrication of layer-by-layer deposition methods. The Laminated Flexible-TENG comprises polytetrafluoroethylene (PTFE) and polymethyl methacrylate (PMMA) films embedded within a flexible and biocompatible polydimethylsiloxane (PDMS) matrix. A nanostructured PDMS surface obtained by oxygen plasma facilitated the sputter deposition of a layered indium tin oxide copper electrode and a tribo-positive PMMA thin layer on top. The addition of the indium tin oxide layer to copper significantly improved the quality and performance of the indium tin oxide-copper electrode. Self-powered Laminated Flexible-TENGs demonstrated impressive pressure-sensing capabilities, featuring dual sensitivity of 7.287 V/kPa for low pressure and 0.663 V/kPa for higher pressure. Moreover, the PDMS-encapsulated TENG sensor effectively traced the physiological motions, such as wrist and finger bending, and efficiently harnessed the waste energy from everyday physical activities, such as walking and jogging. The maximum peak-to-peak voltages of 18.3 and 57.4 V were recorded during these motions. Encapsulated TENGs have broad potential in wearable technology, including healthcare, human-machine interfaces, and energizing microelectronics.

Keywords: Self-powered, biocompatible, wearable sensor, triboelectric nanogenerator (TENG), energy harvesting, human motion monitoring

INTRODUCTION

Wearable electronics have received considerable attention due to their important applications in healthcare monitoring, rehabilitation, human-machine interfaces, and artificial intelligence[1-4]. Flexible and skin-wearable pressure sensors, in particular, have become integral components of wearable devices used in healthcare and physiological motion monitoring[5]. These sensors work by transducing mechanical pressure into electrical signals, such as triboelectricity, piezoelectricity, capacitance, and resistance[6-9]. Among these, the sensors based on triboelectric nanogenerators (TENGs) have gained attention as self-powered devices for dynamic pressure sensing due to their ease of fabrication, a wide choice of materials, cost-effectiveness, and ability to operate efficiently at low frequencies[10,11]. TENGs work on the cooccurrence of triboelectrification and electrostatic induction[12] and are capable of harvesting energy by converting mechanical energy from physiological motions into electrical energy[6,13,14]. Harvesting energy from daily life physical activities, such as walking and jogging, is essentially promising for powering the small-sized electronics[15,16].

Based on basic working modes, TENGs can harvest energy in contact-separation (CS)[17,18], single-electrode[19], linear sliding[20], and freestanding[21] arrangements. The CS mode has been widely studied due to its simple fabrication and compatible design with multi-layer integration[17,18,22]. Fundamentally, in this mode, two dielectric layers of different polarities, namely, tribo-negative and tribo-positive layers, generate surface charges by contact electrification. The charges are then redistributed on the electrodes attached to opposite sides of dielectric layers, which creates a potential difference and flow of charge across the two terminals upon separation of the dielectric layers[22]. The performance of TENG-based sensors has been widely investigated using various fabrication strategies, such as surface texturing, core-shell fiber mats, and surface crumpling, mostly focusing on the tribo-negative materials[23-26]. For example, in the previous work[25], the pressure sensitivities of 1.67 V/kPa (0-3 kPa) and 0.20 V/kPa (3-32 kPa) were reported by enhancing the surface charge potential and charge trapping by polyvinylidene fluoride/silver nanowire nanofibrous membranes. On the other hand, the tribo-positive layer typically has limited choices for flexible TENGs, which would otherwise enable improvements in the performance of these flexible devices[27,28]. Achieving biocompatibility while maintaining the capability for motion monitoring and energy harvesting is another critical issue for wearable devices[29,30]. Furthermore, upholding a high sensitivity across a broad range of pressures is a critical criterion for the sensors in next-generation electronics[31].

In this study, we fabricated a laminated flexible-TENG (LF-TENG) having a dielectric-to-dielectric configuration with a simple fabrication strategy of layer-by-layer deposition. LF-TENGs are composed of polytetrafluoroethylene (PTFE) and polymethyl methacrylate (PMMA) films encapsulated in flexible and biocompatible polydimethylsiloxane (PDMS) for demonstration of motion monitoring and energy harvesting. A textured PDMS substrate was used to deposit the layered indium tin oxide-copper (ITO/Cu) electrode by a sputtering and tribo-positive PMMA thin layer over it. The introduction of the ITO layer onto the layered ITO/Cu electrode significantly improved the overall quality and performance of the electrode. The primary function of the electrode is to efficiently transfer the charges generated within the triboelectric layer to the external circuit while minimizing any losses[32,33]. The LF-TENG displayed decent pressure-sensing capabilities, featuring a pressure sensitivity of 7.287 V/kPa in the low-pressure range (0.0245 to 1.23 kPa) and 0.663 V/kPa in the higher-pressure range (2.45 to 23.3 kPa). Along with the fairly decent self-powered sensing, the LF-TENG also exhibited a high power density of 306.2 mW/m^2. The LF-TENG was then encapsulated between thin layers of PDMS with two acrylic spacers. The encapsulated TENG (E-TENG) sensor effectively traced the physiological motions, such as wrist and finger bending.

Furthermore, the device was utilized for harvesting the waste energy from everyday activities, such as walking and jogging, producing peak-to-peak voltages of 18.3 and 57.4 V during these motions.

EXPERIMENTAL

Materials

The triboelectric materials employed for this study included PMMA (950PMMA A7, K1 solution, Korea) and commercial PTFE films of thickness 100 μm (Marhynchus, China). PDMS (Sylgard 184, Dow Corning Corp) served as the backbone material for the TENG due to its flexibility and biocompatibility, providing the necessary structure for the device. The sputter targets, Cu (diameter = 57 mm, thickness = 1.5 mm) and ITO (diameter = 57 mm, thickness = 1 mm), were purchased from Vacuum Thin Film Materials, Korea. Pressure-sensitive tape (Scotch™ Magic Tape 810) was used as a mold on a glass substrate to control the thickness of PDMS. The commercial silver paste (ELCOAT P-100) was used to connect the tin-plated copper tape terminals (3M 1183) to the electrodes.

Characterization and measurement

The surface modification of PDMS was obtained by reactive ion etching RIE (VITA, Femto Science), allowing for targeted modification of surface properties. A Sputter Coater (Q300T D Plus, Quorum Tech) was used to deposit Cu and ITO to create ITO/Cu electrodes. The surface morphology analysis was conducted utilizing advanced electron microscopy techniques, specifically scanning electron microscopy coupled with energy dispersive X-ray spectroscopy (SEM-EDX), using a Hitachi SU-6600 instrument at an operating voltage of 15 kV. To investigate the electrical response of TENGs as a function of load, frequency, and the gap between upper and lower surfaces, we used a custom-designed tapping device. Tapping was then conducted by adjusting displacement and frequency through a Z-axis motorized stage, controlled by modifying the amplitude and period of sinusoidal waves. Current measurements were meticulously obtained using a high-precision parameter analyzer (Keithley, 4200A). Additionally, capacitor charging voltage measurements were performed by monitoring voltage fluctuations during mechanical tapping. The data was accurately recorded and analyzed using an oscilloscope (Keysight, DSOX1202G). All the electrical measurements were taken at ~60% relative humidity and ~25 °C. Following the acquisition of voltage data through the oscilloscope, a crucial step in our methodology involved post-processing to ensure data accuracy only for the applications involving subtle voltages such as finger bending and wrist bending. To enhance the clarity and precision of the obtained data and discern differences more accurately, a 60 Hz low-pass filter was meticulously applied to filter out electrical noise, refining the figures and aiding in a more nuanced analysis.

Fabrication of LF-TENG

The presented LF-TENG consists of two triboelectric layers. A 100 μm thick PTFE film was selected as the tribo-negative layer owing to its high electronegativity stemming from the presence of fluorine atoms[34]. Meanwhile, a ~1.2 μm thick PMMA layer was utilized as the tribo-positive layer due to its excellent mechanical and wear resistance properties[35]. A ~300 μm thick flexible PDMS layer served as the structural backbone for the tribo-positive PMMA layer.

The fabrication process of LF-TENGs is illustrated in Figure 1A. First, the PDMS base (Sylgard 184A, Dow Corning Corp) and curing agent (Sylgard 184B, Dow Corning Corp) were mixed at a weight ratio of 10:1. The PDMS mixture was degassed and cured at 65 °C for 2.5 h on a glass mold made with a pressure-sensitive tape (Scotch™ Magic Tape 810) to control the thickness of the PDMS film. A 300 μm thick 20 × 20 mm^2 PDMS film was peeled off from the glass mold and treated with oxygen (O_2) plasma in a reactive ion etching (100 W, 20 sccm) chamber for 50 s to obtain the wrinkle-like nanostructures on the PDMS surface. These wrinkle-like nanostructures enhanced the adhesion of electrodes on the PDMS

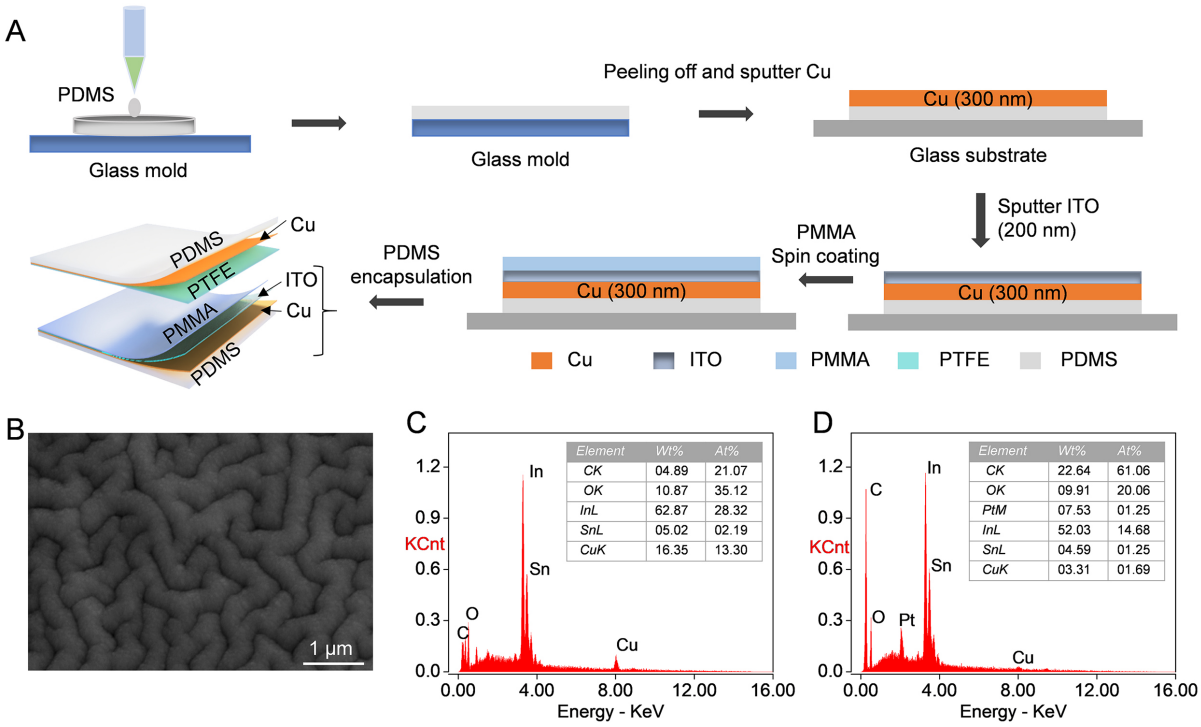

Figure 1. Fabrication of LF-TENG and surface characterization. (A) Schematic diagram of the fabrication of LF-TENG; (B) SEM image of the layered indium tin ITO/Cu electrode sputter deposited on O_2-treated PDMS. The EDX analysis of the elemental composition of the layered ITO/Cu electrode before PMMA spin coating (C) and after spin coating PMMA (D). EDX: Energy dispersive x-ray; ITO/Cu: indium tin oxide-copper; LF-TENG: laminated flexible-triboelectric nanogenerator; PDMS: polydimethylsiloxane; PMMA: polymethyl methacrylate; SEM: scanning electron microscopy.

surface by increasing surface energy and roughness[36]. Supplementary Figure 1A and B shows the scanning electron microscope (SEM) images of pristine and O_2 plasma-treated PDMS (O-PDMS) surfaces, respectively. After that, the O-PDMS film was attached to a glass substrate, and then a 920 nm thick Cu electrode was sputtered (60 mA, 9.8 × 10^{-6} bar, 46 nm/min) on the O-PDMS surface. Subsequently, a 440 nm ITO layer was deposited (40 mA, 5 × 10^{-6} bar, 22 nm/min) on top of the Cu layer. This improved the quality and performance of the electrode by filling in the possible cracks formed during the plasma sputtering on flexible O-PDMS. The cross-sectional SEM image of PMMA coated on the ITO/Cu electrode can be seen in Supplementary Figure 1C. The SEM images and energy dispersive X-ray (EDX) spectra of cracked Cu and ITO-filled Cu are shown in Supplementary Figure 2. Figure 1B shows the SEM image of the ITO/Cu electrode deposited on O-PDMS. A tin-coated copper tape was then pasted using a small amount of commercial silver paste at one corner of the ITO/Cu electrode, which is connected to the negative terminal of an oscilloscope. After that, a thin PMMA layer (~1.2 μm) was coated onto the ITO surface by spin coating the PMMA precursor (2,000 rpm, 30 s) such that the layered ITO/Cu was embedded in PMMA, which was cured at 120 °C for 10 min on a hotplate. The thickness of the PMMA film was measured from SEM imaging [Supplementary Figure 1C]. EDX analysis was conducted on the ITO/Cu electrode to observe the elemental composition before and after PMMA coating. Figure 1C and D shows the elemental count of the ITO/Cu electrode on O-PDMS before and after PMMA spin-coating, respectively. It was observed that the Cu layer was actually embedded under the ITO layer. To compare the performance of voltage and current generation of LF-TENGs with and without ITO layers, a control sample without the ITO layer was also fabricated, and its output performance will be discussed in the later section.

On the other hand, for tribo-negative layers, a 920 nm thick Cu electrode was sputtered on the top of a 100 μm thick PTFE film. After pasting the tin-plated copper tape onto the Cu electrode, the surface was coated by spin coating 100 μm thick PDMS, which was cured at 65 °C for 2.5 h. Finally, the LF-TENG, as shown in Figure 1A, was assembled to test the cyclic performance. It was encapsulated in two pieces of (30 by 40 mm^2) 0.3 mm thick PDMS to create a sensor for monitoring human motion. Before encapsulation, a 1 mm thick acrylic spacer was inserted along both edges to form a gap between the PTFE and PMMA surfaces. The encapsulated LF-TENG is represented as an E-TENG hereafter.

RESULTS AND DISCUSSION

Working mechanism and cyclic performance

Figure 2A represents the working mechanism of LF-TENGs based on CS modes. In the initial state, the two triboelectric layers are separated with no surface charges. When the triboelectric surfaces come into contact through mechanical force, the surface charges are generated through contact electrification (I). The PTFE surface will be negatively charged, and the PMMA surface will possess positive charges. The charges are then redistributed on the electrode of PTFE and PMMA layers, and a potential difference is created across the two terminals[12]. Upon separation of the two surfaces (II), the electrons start to flow through the external circuit to achieve new electrostatic equilibrium until full separation[11,37]. A potential difference equivalent to open circuit voltage is established, which can be expressed as:

$$V_{OC} = \frac{\sigma d}{\varepsilon_0} \quad (1)$$

Where σ is the transferred triboelectric charge density, ε_0 is the vacuum permittivity, and d is the gap distance between triboelectric layers. There is no flow of electrons in fully separated mode (III). Finally, the PTFE surface comes back in contact with the PMMA surface to complete the cycle (IV). The electrons flow back through the external circuit, and the new working cycle begins.

Since the voltage output of LF-TENG mainly depends on the triboelectric charge density of contacting materials, as represented by Equation 1, it is important to carefully select the materials for contact electrification. Supplementary Table 1 shows the triboelectric series of some commonly used materials according to the tendency of accepting electrons (tribo-negative) to donating electrons (tribo-positive). When two materials are far apart on the triboelectric series, more charge transfer occurs. As expected, when the PTFE film (tribo-negative layer) was tested with a pristine PDMS film as a counter triboelectric layer, the output voltage of TENG decreased five times that of PMMA [Supplementary Figure 3]. Figure 2B shows the representative voltage signals generated during a working cycle of LF-TENGs. The response time of LF-TENGs (~20 ms) was obtained from the rise of voltage during II and IV.

A custom-built mechanical tapping device used for the investigation of cyclic performance of our LF-TENG is shown in Figure 2C. As the device starts to reciprocate, an alternating voltage is generated, which is recorded using an oscilloscope. The frequency of tapping was set at 4 Hz, and tapping force (F) was obtained by the load measuring system. The open circuit voltage of LF-TENG is shown as a function of gap distance (d = 2 to 5 mm) in Figure 2D. In order to determine the optimum operating conditions of the TENG as an energy harvesting device, the dependency of output voltage was investigated as a function of the frequency of mechanical tapping ranging from 1 to 4 Hz[38] [Figure 2E]. The peak-to-peak voltage output increased from 14 to 52 V at the tapping frequency of 1 to 4 Hz when d and F were set as 5 mm and 6.3 N, respectively. This was attributed to the increased flow rate of triboelectric charges at higher frequencies[39]. The cyclic voltage output as a function of tapping frequencies at gap distances of 2 to 5 mm (F = 6.3 N) is provided in supporting information [Supplementary Figure 4].

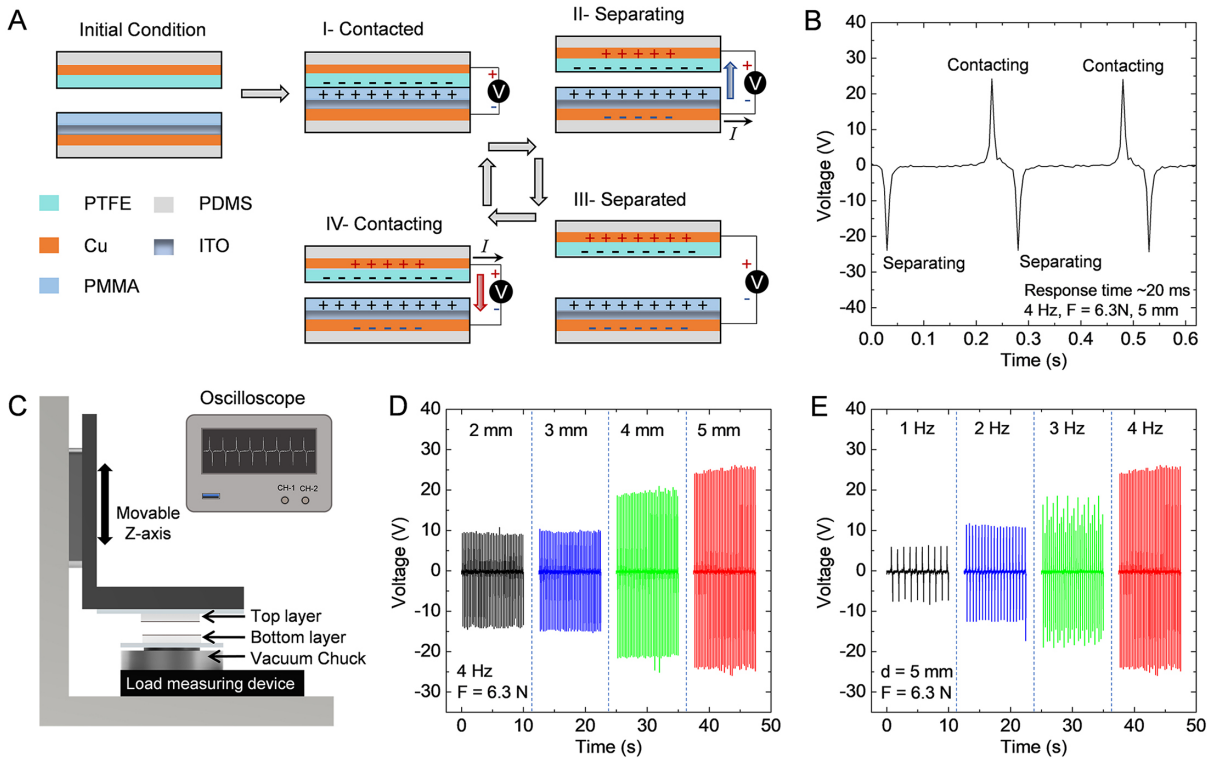

Figure 2. Cyclic performance evaluation of LF-TENG. (A) Working mechanism of LF-TENGs based on CS modes; (B) Representative voltage output of LF-TENGs based on CS modes; (C) Schematic diagram of mechanical tapping device used for the cyclic performance evaluation of LF-TENGs. The top layer (PTFE) is attached to a glass substrate fixed on the movable clamp, and the bottom layer (PMMA) is affixed to the vacuum chuck over a load-measuring unit. The voltage output was recorded by an oscilloscope; (D) Voltage output of LF-TENG as a function of separation gap (d = 2, 3, 4, and 5 mm) when the tapping frequency and force are fixed at 4 Hz and 6.3 N; (E) Voltage output of LF-TENG as a function of tapping frequency (1, 2, 3, and 4 Hz) at d = 5 mm and F = 6.3 N. CS: Contact-separation; LF-TENG: laminated flexible-triboelectric nanogenerator; PMMA: polymethyl methacrylate; PTFE: polytetrafluoroethylene.

Figure 3A compares the open circuit voltage of LF-TENG, which has an ITO/Cu bottom electrode embedded in PMMA, with a control sample (without an ITO layer on the bottom electrode). The voltage output was obtained at a tapping frequency of 4 Hz and force of 6.3 N, while the separation gap was fixed as 5 mm. It was observed that the LF-TENG with ITO layer on the bottom electrode showed an 85.7% rise in voltage output. A bridge rectifier was used to convert alternating current to direct current [Figure 3B]. Figure 3C illustrates the rectified current of LF-TENG and the control sample. For both samples, the current was measured by manually tapping the top layer (PTFE) on the bottom layer (PMMA). The rectified current of LF-TENG was measured to be 400% higher than that of TENG without an ITO layer on the bottom electrode. The ability of charge collection of the bottom Cu electrode was improved when a thin layer (~440 nm) of ITO was sputtered on it since the ITO can fill in the cracks formed on the Cu electrode deposited on O-PDMS, thereby improving the electrical conductivity from 8.70 to 75.8 S/m.

To further investigate the energy harvesting performance of LF-TENG, the rectified voltage and current were measured at various Ohmic loads ranging from 1 kΩ to 2 GΩ. The voltage increased with increasing load while the current decreased due to the high ohmic losses [Figure 3D]. At first, the current slightly decreased in the range of 1 kΩ to 1 MΩ since the charge transfer was rather similar to the short circuit condition. However, the charge transfers notably decreased from 1 MΩ to 2 GΩ, resulting in diminished current output. The output of LF-TENG is close to the current open circuit condition[12]. The rectified current data at various ohmic loads is presented in Supplementary Figure 5. The electronic devices have

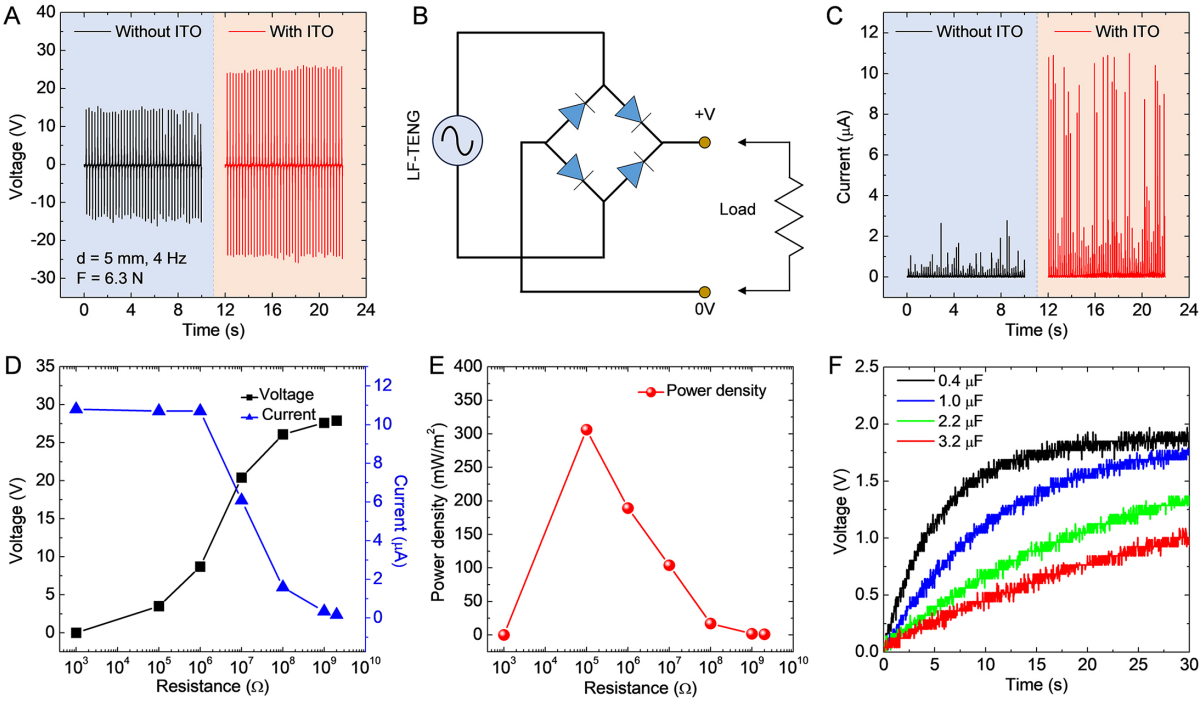

Figure 3. Output performance of LF-TENG with ITO layer on Cu electrode and without ITO layer (control sample). (A) The comparison of LF-TENG voltage output with ITO layer on Cu electrode and without ITO layer (control sample); (B) Bridge rectifier circuits used to convert the AC to DC; (C) The comparison of LF-TENG DC output with ITO layer on Cu electrode and without ITO layer (control sample); (D) Output voltage and current at ohmic loads of 1 kΩ to 2 GΩ; (E) Power density ($P = V^2/RA$), where V, R, and A are the voltage, resistance, and contact area of LF-TENGs, respectively; (F) Charging voltage of 0.4, 1.0, 2.2, and 3.2 μF capacitors. AC: Alternating current; DC: direct current; ITO: indium tin oxide; LF-TENG: laminated flexible-triboelectric nanogenerator.

finite impedance values when the LF-TENG is actually employed as an energy harvester. Therefore, it is crucial to determine the ideal resistance value that can efficiently power the electronics by practically using the LF-TENG. Figure 3E illustrates that the maximum electrical power density reached 306.2 mW/m² when the resistance was set to 100 kΩ. The ability of 20 × 20 mm² LF-TENG was then investigated for charging the commercial capacitors of 0.4, 1.0, 2.2, and 3.2 μF equivalent capacitances. The energy harvested by LF-TENG operating at a 5 mm separation gap (F = 6.3 N, 4 Hz) was utilized to charge the capacitors through a bridge rectifier circuit. Figure 3F shows that within a 30-second timeframe, the charging voltages of 0.4, 1.0, 2.2, and 3.2 μF capacitors reached up to 1.96, 1.78, 1.36, and 1.08 V, respectively.

Pressure and tactile sensing

The relationship between voltage response and tapping force was investigated for the application of LF-TENG for pressure sensing. Figure 4A illustrates the voltage output as the tapping force varied from 0.0098 to 9.32 N. Clearly, as the tapping force increases, so does the voltage output. This can be attributed to the fact that the actual contact area between the triboelectric layers is enhanced with greater tapping force, as the surface roughness of these layers hinders full contact at lower pressures[40]. Figure 4B presents the corresponding pressure sensitivity, which was obtained by linear fitting the positive peak of open circuit voltage and tapping pressure ($S = \Delta V/\Delta p$). The findings in Figure 4B indicate that the LF-TENG demonstrated a higher sensitivity of 7.287 V/kPa within the low-pressure range (0.0245 to 1.23 kPa). This was primarily due to the gradually increasing contact area between the triboelectric layers with the tapping force, which could be attributed to the surface roughness induced by a wrinkle-like structure of the PDMS backbone. However, this sensitivity declined to 0.663 V/kPa within the range of 2.45 to 23.3 kPa when the

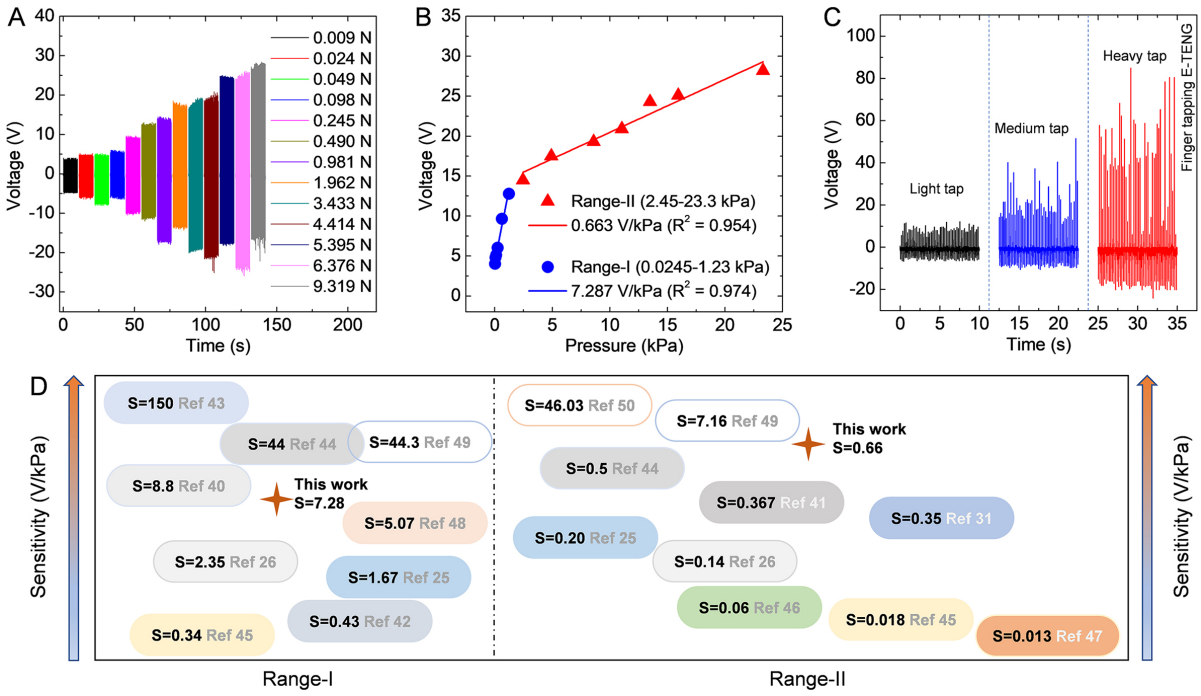

Figure 4. Pressure-sensitive voltage response. (A) Tapping force-dependent voltage response of LF-TENG; (B) Pressure sensitivity of LF-TENG sensors in range-I (0.0245 to 1.23 kPa) and range-II (2.45 to 23.3 kPa); (C) Finger tapping response of PDMS-encapsulated E-TENG at light, medium, and heavy tapping force; (D) Comparison of LF-TENG pressure sensitivity with other TENG-based pressure sensors[25,26,31,40-50]. E-TENG: Encapsulated-triboelectric nanogenerator; LF-TENG: laminated flexible-triboelectric nanogenerator; PDMS: polydimethylsiloxane.

rise in contact area reached a saturation point. This observation aligns with prior research. For instance, a previously reported TENG in[26] displayed a pressure sensitivity of 2.35 V/kPa for pressures below 1 kPa, but this sensitivity decreased to 0.14 V/kPa at higher pressures.

Additionally, our LF-TENG (20 × 20 mm²) was encapsulated in two pieces of PDMS to create the PDMS-E-TENG sensor to assess its ability for tactile sensing through finger tapping, with variations in tapping force from light to heavy. The voltage produced by E-TENGs remained consistent and increased as the force of finger tapping increased [Figure 4C]. This suggests that the E-TENG sensor reacts consistently to varying levels of tapping force, making it suitable for applications related to tactile sensing with a broad range of pressure sensitivity[41,42]. In comparison to other pressure sensors based on TENGs [Figure 4D and Supplementary Table 2], the LF-TENG exhibits reasonably decent sensitivity across both low and high-pressure ranges, especially when compared with dielectric-to-dielectric configurations, which typically yield higher outputs[25,31,42]. Besides that, E-TENGs can generate a maximum peak-to-peak voltage of 100 V with finger tapping, which demonstrates its strong potential for energy harvesting.

Human motion monitoring and simultaneous energy harvesting

Based on the decent pressure sensing performance shown in the prior section, we employed the PDMS-E-TENG sensor for monitoring human motion. Figure 5A shows the optical images of E-TENG sensors attached to a human wrist and finger for monitoring the movements of wrist extension (upward motion), flexion (downward motion), and finger bending. To ensure effective monitoring, the E-TENG sensor was closely affixed to the body using a pressure-sensitive tape. No signal was detected when the wrist was stationary [Figure 5B]. However, when the wrist started extension and flexion motions, our self-

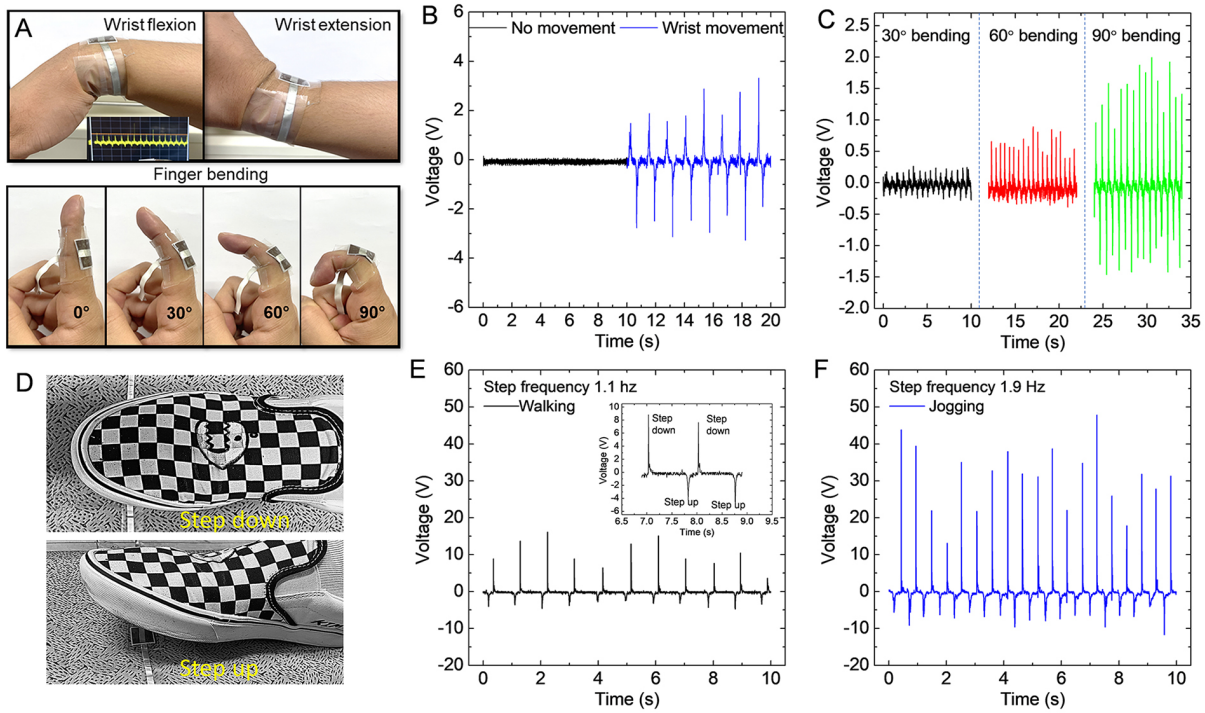

Figure 5. Monitoring motion and energy harvesting. (A) Optical images of E-TENG sensors attached to the human wrist (top) and index finger (bottom) for motion detection; (B) Voltage output signal of wrist movement (extension and flexion); (C) Voltage output signal of finger bending angles of 30°, 60°, and 90°; (D) Demonstration of energy harvesting from walking and jogging motions; (E) Voltage output signal of walking motion at step frequency of 1.1 Hz. Stepping down and up produces the positive and negative peaks (inset); (F) Voltage output signal of jogging motion at step frequency of 1.9 Hz. E-TENG: Encapsulated-triboelectric nanogenerator.

powered E-TENG sensor generated a voltage signal of approximately 2 V. Moreover, the E-TENG sensor can serve as an energy harvesting device simultaneously. E-TENG was further tested for the detection of bending movements of the index finger at approximately 30°, 60°, and 90° angles, respectively [Figure 5C]. These bending movements of the finger can be clearly traced by the distinctive voltage signals of approximately 0.188, 0.889, and 1.99 V for 30°, 60°, and 90° angles, respectively.

Moreover, everyday physical activities, such as walking and jogging, can serve as valuable energy sources for the E-TENG sensor. In Figure 5D, we demonstrate using the E-TENG sensor for energy harvesting during walking and jogging motions. To capture these motions, individuals stepped onto the E-TENG sensor. The voltage signals produced during these activities [Figure 5E and F] can be easily distinguished based on their amplitudes and frequencies. When stepping down on the floor, the E-TENG sensor was compressed, resulting in positive voltage signals, while stepping up released the sensor, generating negative voltage [Figure 5E, inset]. This behavior aligns with the working mechanism illustrated in Figure 2A. Notably, the E-TENG generated maximum peak-to-peak voltages of 18.3 and 57.4 V during walking and jogging activities, respectively. Simultaneously, the frequencies of walking and jogging were recorded at 1.1 and 1.9 Hz, respectively. Given their high power density and superior sensitivity in a broad pressure range, E-TENGs demonstrate significant potential for applications such as human motion monitoring, tactile sensing, and harvesting the waste energy from daily life physical activities.

CONCLUSIONS

In summary, the LF-TENG, specifically in a dielectric-to-dielectric configuration with PTFE as the tribo-negative layer and PMMA as the tribo-positive layer, exhibited promising characteristics for pressure sensing and energy harvesting applications. The working mechanism of LF-TENGs based on the CS mode was evaluated, demonstrating the generation of a maximum peak-to-peak open-circuit voltage of 52 V when subjected to mechanical tapping at a low frequency of 4 Hz. Notably, the introduction of an ITO layer on a Cu electrode deposited on a flexible PDMS substrate improved the electrode quality, resulted in significantly enhanced voltage output and charge collection efficiency. The LF-TENG with an ITO/Cu electrode showed a high-power density of 306.2 mW/m^2. Moreover, the LF-TENG exhibited remarkable pressure sensing capabilities, featuring a sensitivity of 7.287 V/kPa within the lower pressure range (0.0245 to 1.22 kPa) and 0.663 V/kPa in the higher-pressure range (2.45 to 23.3 kPa). This dual-range pressure sensitivity enables our E-TENG to be highly responsive to a wide spectrum of finger-tapping forces, rendering it well-suited for tactile and pressure sensing applications. This versatility was extended to human motion monitoring, where the E-TENG sensor effectively detected wrist and finger movements and even harnessed energy from everyday physical activities such as walking and jogging. The E-TENG generated the maximum peak-to-peak voltages of 18.3 and 57.4 V during walking and jogging activities, respectively. With its high-power density and sensitivity, the E-TENG holds great promise for diverse applications, including tactile and pressure sensing, healthcare monitoring and rehabilitation, and human-machine interface.

DECLARATIONS

Authors' contributions

Conceptualization: Jan AA, Kim S (Seok Kim)
Tapping machine Software: Kim S (Seungbeom Kim)
Formal analysis: Jan AA, Kim S (Seungbeom Kim)
Methodology, writing - original draft preparation, writing - review and editing: Jan AA, Kim S (Seungbeom Kim), Kim S (Seok Kim)

Availability of data and materials

Data is available upon request from the corresponding author.

Financial support and sponsorship

This work was supported by the National Research Foundation of Korea (NRF), funded by the Ministry of Science and ICT (2022M317A3050820; 2022R1A4A3033320; 2022R1A2C3006420).

Conflicts of interest

All authors declared that there are no conflicts of interest.

Ethical approval and consent to participate

According to the Korea National Institute for Bioethics Policy, under the Human Subject Research Division, enforcement rule article 13 states that research using only simple contact measuring equipment or observation equipment that does not cause physical changes is exempt from IRB approval. Our work involves simply placing the device on the skin, which does not physically affect humans. Therefore, we do not require IRB approval. All participants participated in the experiment with informed consent.

Consent for publication

Not applicable.

REFERENCES

1. Trung TQ, Lee NE. Flexible and stretchable physical sensor integrated platforms for wearable human-activity monitoringand personal healthcare. *Adv Mater* 2016;28:4338-72. DOI PubMed
2. Guo Y, Zhong M, Fang Z, Wan P, Yu G. A wearable transient pressure sensor made with MXene nanosheets for sensitive broad-range human-machine interfacing. *Nano Lett* 2019;19:1143-50. DOI
3. Chen L, Lu M, Yang H, et al. Textile-based capacitive sensor for physical rehabilitation *via* surface topological modification. *ACS Nano* 2020;14:8191-201. DOI
4. Shen S, Yi J, Sun Z, et al. Human machine interface with wearable electronics using biodegradable triboelectric films for calligraphy practice and correction. *Nano Lett* 2022;14:225. DOI PubMed PMC
5. Wang Y, Zhu W, Deng Y, et al. Self-powered wearable pressure sensing system for continuous healthcare monitoring enabled by flexible thin-film thermoelectric generator. *Nano Energy* 2020;73:104773. DOI
6. Wang J, Li S, Yi F, et al. Sustainably powering wearable electronics solely by biomechanical energy. *Nat Commun* 2016;7:12744. DOI PubMed PMC
7. Wang Y, Yu Y, Wei X, Narita F. Self-powered wearable piezoelectric monitoring of human motion and physiological signals for the postpandemic era: a review. *Adv Mater Technol* 2022;7:2200318. DOI
8. Nie B, Li R, Cao J, Brandt JD, Pan T. Flexible transparent iontronic film for interfacial capacitive pressure sensing. *Adv Mater* 2015;27:6055-62. DOI PubMed
9. Zhang Y, Hu Y, Zhu P, et al. Flexible and highly sensitive pressure sensor based on microdome-patterned PDMS forming with assistance of colloid self-assembly and replica technique for wearable electronics. *ACS Appl Mater Interfaces* 2017;9:35968-76. DOI
10. Win Zaw NY, Yun J, Goh TS, et al. All-polymer waterproof triboelectric nanogenerator towards blue energy harvesting and self-powered human motion detection. *Energy* 2022;247:123422. DOI
11. Xia X, Zhou Z, Shang Y, Yang Y, Zi Y. Metallic glass-based triboelectric nanogenerators. *Nat Commun* 2023;14:1023. DOI PubMed PMC
12. Niu S, Wang S, Lin L, et al. Theoretical study of contact-mode triboelectric nanogenerators as an effective power source. *Energy Environ Sci* 2013;6:3576-83. DOI
13. Kim KN, Kim SY, Choi SH, et al. All-printed wearable triboelectric nanogenerator with ultra-charged electron accumulation polymers based on MXene nanoflakes. *Adv Electron Mater* 2022;8:2200819. DOI
14. Lai YC, Deng J, Zhang SL, Niu S, Guo H, Wang ZL. Single-thread-based wearable and highly stretchable triboelectric nanogenerators and their applications in cloth-based self-powered human-interactive and biomedical sensing. *Adv Funct Mater* 2017;27:1604462. DOI
15. Yang W, Chen J, Zhu G, et al. Harvesting energy from the natural vibration of human walking. *ACS Nano* 2013;7:11317-24. DOI
16. Xing F, Jie Y, Cao X, Li T, Wang N. Natural triboelectric nanogenerator based on soles for harvesting low-frequency walking energy. *Nano Energy* 2017;42:138-42. DOI
17. Zi Y, Wu C, Ding W, Wang ZL. Maximized effective energy output of contact-separation-triggered triboelectric nanogenerators as limited by air breakdown. *Adv Funct Mater* 2017;27:1700049. DOI
18. Chu Y, Cao Z, Xu J, et al. Theoretical study of nanogenerator with resistive load and its sensing performance as a motion sensor. *Nano Energy* 2021;81:105628. DOI
19. Niu S, Liu Y, Wang S, et al. Theoretical investigation and structural optimization of single-electrode triboelectric nanogenerators. *Adv Funct Mater* 2014;24:3332-40. DOI
20. Niu S, Liu Y, Wang S, et al. Theory of sliding-mode triboelectric nanogenerators. *Adv Mater* 2013;25:6184-93. DOI
21. Jiang T, Chen X, Han CB, Tang W, Wang ZL. Theoretical study of rotary freestanding triboelectric nanogenerators. *Adv Funct Mater* 2015;25:2928-38. DOI
22. Chu Y, Han R, Meng F, et al. Theoretical study on the output of contact-separation triboelectric nanogenerators with arbitrary charging and grounding conditions. *Nano Energy* 2021;89:106383. DOI
23. Wang J, Qian S, Yu J, et al. Flexible and wearable PDMS-based triboelectric nanogenerator for self-powered tactile sensing. *Nanomaterials* 2019;9:1304. DOI PubMed PMC
24. Chang KB, Parashar P, Shen LC, et al. A triboelectric nanogenerator-based tactile sensor array system for monitoring pressure distribution inside prosthetic limb. *Nano Energy* 2023;111:108397. DOI
25. Lou M, Abdalla I, Zhu M, Yu J, Li Z, Ding B. Hierarchically rough structured and self-powered pressure sensor textile for motion sensing and pulse monitoring. *ACS Appl Mater Interfaces* 2020;12:1597-605. DOI
26. Cao Y, Guo Y, Chen Z, et al. Highly sensitive self-powered pressure and strain sensor based on crumpled MXene film for wireless human motion detection. *Nano Energy* 2022;92:106689. DOI
27. Kim DW, Lee JH, Kim JK, Jeong U. Material aspects of triboelectric energy generation and sensors. *NPG Asia Mater* 2020;12:6. DOI
28. Ryu H, Lee JH, Kim TY, et al. High-performance triboelectric nanogenerators based on solid polymer electrolytes with asymmetric pairing of ions. *Adv Energy Mater* 2017;7:1700289. DOI
29. Sang M, Kim K, Shin J, Yu KJ. Ultra-thin flexible encapsulating materials for soft bio-integrated electronics. *Adv Sci* 2022;9:2202980. DOI PubMed PMC
30. Kim NI, Lee JM, Moradnia M, et al. Biocompatible composite thin-film wearable piezoelectric pressure sensor for monitoring of physiological and muscle motions. *Soft Sci* 2022;2:8. DOI

31. Rasel MS, Maharjan P, Salauddin M, et al. An impedance tunable and highly efficient triboelectric nanogenerator for large-scale, ultra-sensitive pressure sensing applications. *Nano Energy* 2018;49:603-13. DOI
32. Aazem I, Mathew DT, Radhakrishnan S, et al. Electrode materials for stretchable triboelectric nanogenerator in wearable electronics. *RSC Adv* 2022;12:10545-72. DOI PubMed PMC
33. Jo S, Kim I, Jayababu N, Kim D. Performance-enhanced triboelectric nanogenerator based on the double-layered electrode effect. *Polymers* 2020;12:2854. DOI PubMed PMC
34. Xing C, Tian Y, Yu Z, Li Z, Meng B, Peng Z. Cellulose nanofiber-reinforced MXene membranes as stable friction layers and effective electrodes for high-performance triboelectric nanogenerators. *ACS Appl Mater Interfaces* 2022;14:36741-52. DOI
35. Busolo T, Ura DP, Kim SK, et al. Surface potential tailoring of PMMA fibers by electrospinning for enhanced triboelectric performance. *Nano Energy* 2019;57:500-6. DOI
36. Maji D, Das S. Analysis of plasma-induced morphological changes in sputtered thin films over compliant elastomer. *J Phys D Appl Phys* 2014;47:105401. DOI
37. Han J, Wang Y, Ma Y, Wang C. Enhanced energy harvesting performance of triboelectric nanogenerators via dielectric property regulation. *ACS Appl Mater Interfaces* 2023;15:31795-802. DOI
38. Zhu G, Peng B, Chen J, Jing Q, Lin Wang Z. Triboelectric nanogenerators as a new energy technology: from fundamentals, devices, to applications. *Nano Energy* 2015;14:126-38. DOI
39. Tantraviwat D, Buarin P, Suntalelat S, et al. Highly dispersed porous polydimethylsiloxane for boosting power-generating performance of triboelectric nanogenerators. *Nano Energy* 2020;67:104214. DOI
40. Garcia C, Trendafilova I, Guzman de Villoria R, Sanchez del Rio J. Self-powered pressure sensor based on the triboelectric effect and its analysis using dynamic mechanical analysis. *Nano Energy* 2018;50:401-9. DOI
41. He J, Xie Z, Yao K, et al. Trampoline inspired stretchable triboelectric nanogenerators as tactile sensors for epidermal electronics. *Nano Energy* 2021;81:105590. DOI
42. Lin MF, Xiong J, Wang J, Parida K, Lee PS. Core-shell nanofiber mats for tactile pressure sensor and nanogenerator applications. *Nano Energy* 2018;44:248-55. DOI
43. Liu Z, Zhao Z, Zeng X, Fu X, Hu Y. Expandable microsphere-based triboelectric nanogenerators as ultrasensitive pressure sensors for respiratory and pulse monitoring. *Nano Energy* 2019;59:295-301. DOI
44. Zhu G, Yang WQ, Zhang T, et al. Self-powered, ultrasensitive, flexible tactile sensors based on contact electrification. *Nano Lett* 2014;14:3208-13. DOI
45. Zhao Z, Huang Q, Yan C, et al. Machine-washable and breathable pressure sensors based on triboelectric nanogenerators enabled by textile technologies. *Nano Energy* 2020;70:104528. DOI
46. Wang X, Zhang H, Dong L, et al. Self-powered high-resolution and pressure-sensitive triboelectric sensor matrix for real-time tactile mapping. *Adv Mater* 2016;28:2896-903. DOI
47. Pu X, Liu M, Chen X, et al. Ultrastretchable, transparent triboelectric nanogenerator as electronic skin for biomechanical energy harvesting and tactile sensing. *Sci Adv* 2017;3:e1700015. DOI PubMed PMC
48. Rao J, Chen Z, Zhao D, et al. Tactile electronic skin to simultaneously detect and distinguish between temperature and pressure based on a triboelectric nanogenerator. *Nano Energy* 2020;75:105073. DOI
49. Zhong Y, Wang J, Han L, et al. High-performance flexible self-powered triboelectric pressure sensor based on chemically modified micropatterned PDMS film. *Sens Actuator A Phys* 2023;349:114013. DOI
50. Zheng Z, Yu D, Wang B, Guo Y. Ultrahigh sensitive, eco-friendly, transparent triboelectric nanogenerator for monitoring human motion and vehicle movement. *Chem Eng J* 2022;446:137393. DOI